

THE INFLUENCE OF QUENCH RATE ON THE MECHANICAL BEHAVIOUR OF AA6082

N. Sarmady¹, N.C. Parson², Mei Li³, and W. J. Poole¹

*¹ Department of Materials Engineering, University of British Columbia
Vancouver, BC, Canada*

*² Rio Tinto Aluminium
Jonquière QC, Canada*

*³ Ford Motor Company
Dearborn, Michigan, USA*

ABSTRACT

The mechanical behaviour of AA6082 is a function of the extrusion conditions and in particular, the quench rate after extrusion. It is well known that precipitation of Mg-Si phases on grain boundaries during quenching can negatively affect the ductility of the alloy. In this study, AA6082 alloys containing 0.5 wt. % Mn and 0.15 wt. % Cr were direct chill (DC) cast, homogenized and then extruded to produce 3 mm x 42 mm strips. The microstructure in the as-extruded strips was unrecrystallized due to the Zener-Smith drag from the Mn/Cr dispersoids. It was shown that a solution treatment of 5 minutes at 560°C did not significantly affecting the as-extruded microstructure but if the as-extruded strip was cold rolled prior to heating, recrystallization occurred concurrently with the solution treatment. As such, 3 initial microstructures were produced, i.e. unrecrystallized and recrystallized with a grain size of 9 and 40 µm. After the solution treatment, controlled cooling experiments were conducted using the Gleeble 3500 thermomechanical simulator with cooling rates of 10, 25, 80°C/s as well as water quenched. The mechanical properties (e.g. yield stress, fracture stress and fracture strain) were determined from tensile tests for the different combinations of initial microstructure and cooling rate. The relationship between the quench rate and precipitation of Mg-Si phases on grain boundaries was examined by FEG-SEM. It was found that the yield stress decreased as the cooling rate decreased and that there was complex relationship between the fracture properties and the microstructure.

KEYWORDS

AA6082, Quench sensitivity, Precipitation, Mg-Si phases, Mechanical behaviour

INTRODUCTION

As the automotive industry strives to reduce fuel consumption and CO₂ emissions with the goal of reducing the environmental impact, there is a need for lighter vehicles. As a result, aluminum alloys are gaining popularity to replace steel parts as structural components. An exemplar of this is the Ford F-150 pickup truck which has an aluminum body and is ≈ 750 pounds lighter than the previous steel version of the vehicle. The structure includes a mix of aluminum sheet, extrusions and cast alloys. The current research is concerned with the performance of aluminum extrusions in applications such as side rails, crash tubes and other structural parts. These components experience a combination of bending, stretching and folding both during the forming of the part and in service, e.g. crash of a vehicle. There is a need to have detailed information on the influence of processing on final material performance, in particular the cooling rate after extrusion.

The most commonly used aluminum alloys used in the extruded form are the 6000 series alloys. These alloys offer a good combination of final mechanical properties such as strength and ductility and they have a reasonable processing window which allows for the production of complex profiles at relatively high extrusion speeds. In addition, it is most common to combine the solution heat treatment (i.e. the dissolution of Mg and Si into a solid solution) with the extrusion process, reducing the number of processing steps required. It is, thus, important to consider the cooling rate after extrusion as there is a trade-off between maintaining the maximum amount of Mg and Si in solid solution to achieve the maximum strength during subsequent artificial ageing (i.e. requiring a high cooling rate) and shape control/equipment capabilities which is favoured by lower cooling rate. It is well known that there is a strong interaction between the microstructure and the heterogeneous precipitation of Mg-Si phases during cooling (Strobel et al., 2011). Common nucleation sites include grain boundaries and dispersoids (Lodgaard & Ryum 2000). The control of microstructure and precipitation during cooling is important because it will affect mechanical properties of the final parts, both in terms of the strength (Milkereit & Starink, 2015) and the ductility (Dowling & Martin 1976). In particular, controlling the quench rate after solution treatment is one of the key parameters of interest as it's been shown that it can determine the amount of precipitation of Mg-Si phases along grain boundaries which influences the formability and ductility of the alloys (Vasudevan & Doherty 1987).

The aim of this study is to measure the effect of cooling rate on mechanical properties (both strength and ductility) for an AA6082 extrusion alloy. The role of microstructure will be examined by processing the material to produce i) an unrecrystallized alloy and two recrystallized alloys with a fine (≈ 10 μm) and medium (40 μm) grain size. The strength will be characterized by the yield stress and the ductility by the true fracture stress and true fracture strain as measured in a uniaxial tensile test. Qualitative observations on the precipitation of Mg-Si phases during cooling were made with a field emission gun scanning electron microscope (FEGSEM).

EXPERIMENTAL METHODOLOGY

The aluminum billets were DC cast with a diameter of 100 mm by Rio Tinto Aluminium in Jonquiere, Quebec. The chemical composition of the AA6082 alloy as measured by optical emission spectroscopy (OES) is listed in Table 1. The billets were homogenized for 2 h at 550°C to produce a high volume fraction of dispersoids. The recent work of Liu measured the radius of the dispersoids to be 37 nm and estimated their volume fraction to be 1.3% for this homogenization practice (Liu, 2017).

Table 1. Chemical composition of as-received alloy (%)

Alloy	Mg	Si	Mn	Cr	Fe
0.5Mn 0.14Cr	0.69	1.03	0.5	0.14	0.21

The homogenized billets were extruded on a laboratory scale extrusion press with an initial billet temperature of 500°C and a ram speed of 8 mm/s to produce a strip with dimensions of 42 mm by 3 mm. To study the effect of initial grain structure, some samples were cold rolled using a laboratory scale rolling mill. The aim was to achieve a fine recrystallized grain size of ≈ 10 μm as well as a larger recrystallized grain size

of around 50 μm . After some trial and error experiments, it was found that if the samples were solution treated for 5 minutes at 560°C in the salt bath and then cold rolled by 30 or 80%, a small and larger recrystallized grain size would be obtained after the subsequent solution treatment.

To study the effect of cooling rate on precipitation, all samples were solution treated at 560°C for 5 minutes to re-dissolve Mg and Si into solid solution in either a salt bath (for water quench or air cooled samples) or using the Gleeble 3500 thermomechanical simulator. The Gleeble samples were 12 mm \times 82 \times 3 mm strips, small enough to fit inside the Gleeble without there being any compressive forces on the sample during heating, and large enough to be able to machine them into the 66 mm long tensile testing samples that had previously been used. The sample geometry for the Gleeble sample used is shown in Figure 1.

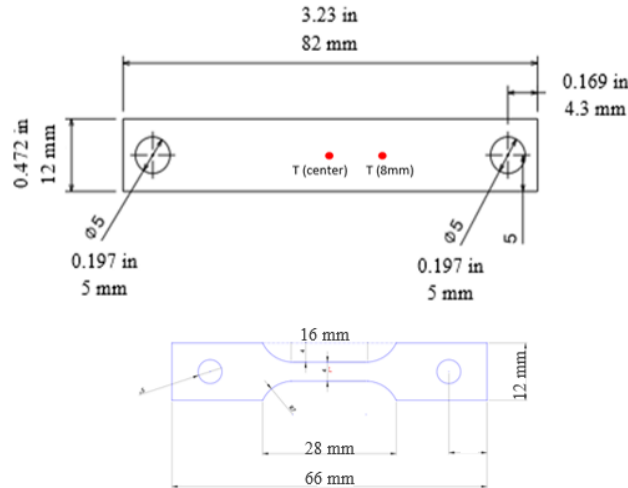


Figure 1. Gleeble and tensile test sample geometry

The sample was held at each end by stainless steel grips. To conduct this test, a set of K-type thermocouples were first spot welded to the center of the sample and at ± 8 mm from the centre to ensure that the temperature was uniform along the sample, i.e. since the gauge length of the tensile sample was 16 mm. Prior to heating the sample, the chamber was pumped down to a vacuum of approximately 3.5×10^{-1} Torr. The tank was then back filled with argon to a pressure of 10 kPa. The heating rate was programmed to be 5°C/s to 530°C, and then a slower heating rate of 0.5°C/s to 560°C to minimize failure of the spot welded thermocouples to the aluminum sample. The quench itself was conducted with helium gas flowing at the various pressures to achieve the different quench rates as shown in Table 2. Note that these were the starting pressures and they were manually adjusted during the quench to ensure steady power input from the Gleeble.

Table 2. Helium gas pressure to use for desired quench rates

Quench Rate	10°C/s	25°C/s	80/s
He Gas Pressure	2 Psi	6 Psi	40 Psi

After cooling, the samples were artificially aged at 180°C for 4 hours in an oil bath to obtain the peak strength (T6 temper). A schematic diagram of the heat treatment is shown in Figure 2.

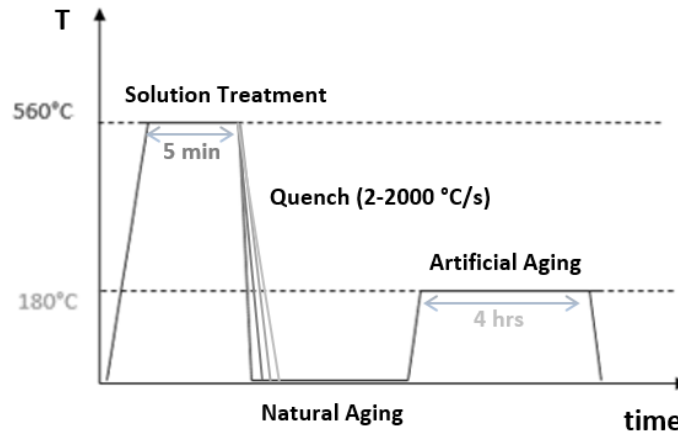


Figure 2. Heat treatment cycle (temperature vs. time)

Samples for metallographic observations were sectioned from the center of the extrusion in 10 mm x 10 mm sections and were polished using 600 grit paper for 2 minutes, 800 grit for 5 minutes, and 1200 grit paper until all visible scratches were removed from the surface. They were then polished using a 1 μ m Texmet cloth along with diamond suspension and a microid diamond compound extender as lubricant, for 15 minutes or until scratches visible under the optical microscope had been removed. Finally, 0.05 μ m Chemotexile® cloth was used along with Colloidal Silica for \approx 10 minutes until the surface was smooth and reflective. A Zeiss FEG-SEM was used to collect images of the samples using the secondary electron (SE) mode. The Mn/Cr containing constituent particles and dispersoids were visible in the SEM at a magnification of 10,000X and the effects of the cooling rate on precipitation of Mg-Si phases were qualitatively examined. For this analysis, the sample surface was etched for 30 seconds using an etchant containing 150 mL Nitric acid diluted with 350 mL methanol which was placed in a metal beaker and connected to a power supply set to a voltage of 9 V. This beaker was placed in a larger beaker containing liquid nitrogen and cooled to -20 °C. Electron Backscatter Diffraction (EBSD) maps were collected to study the grain structure and crystallographic texture of the samples after solution treatment. Samples were prepared similar to the ones for SEM imaging and the Zeiss Sigma FEG-SEM with an EDAX DigiView IV EBSD Camera and EDAX TSL Orientation Imaging Microscopy (OIMTM) Data Collection software.

To quantify how the quench rate affects the mechanical properties, a series of tensile tests were conducted on the sample after artificial ageing, i.e. in the T6 temper. Prior to tensile testing, it is noted that a thin surface layer of approximately 30 μ m of coarse grains of the sample were removed by etching with a 100 g NaOH/L distilled water solution. This surface removal was done by leaving the sample in the solution at a temperature of 50–60°C, for \approx 20–50 minutes. Note that the amount of time required is dependent on the thickness of the coarse grain layer. For example the as extruded samples were left for 50 minutes, whereas the 30% cold rolled samples needed only 20 minutes as the coarse grain layer was thinner.

The tensile testing itself was done with an Instron screw driven machine using the sample geometry shown in Figure 1. A load cell of 5 kN capacity and a extensometer with a gauge length of 12.5 mm were used to collect the load and displacement data. From this, the true stress and strain were calculated in the usual manner. In addition, the true fracture stress (σ_T) and true fracture strain (ε_T) were also calculated using Equations (1) and (2) based on the final fracture areas obtained by SEM images.

$$\sigma_T = F_{fracture} / A_{final} \quad (1)$$

$$\varepsilon_T = \ln(A_{final} / A_{initial}) \quad (2)$$

RESULTS

This section summarizes the results for microstructural characterization and mechanical properties. This includes the Gleeble and tensile test results, as well as characterization of precipitation of Mg_2Si within or along the grain boundaries using the FEGSEM.

Initial Grain Structures

Figure 3a and 4a illustrate the EBSD maps and 001, 111 and 110 pole figures for the grain structure after extrusion, respectively. The grains are highly elongated with subgrains within the grains and exhibit a crystallographic texture typical of plane strain deformation. The average subgrain size was $3.4 \mu m$. Figures 3b and 4b show the grain structure and crystallographic texture after the solution treatment for 5 minutes at $560^\circ C$. It was observed that there was minimal change in the grain structure, both the subgrain size and the texture, after the solution treatment. On the other hand, for the samples which were cold rolled 30 and 80%, recrystallization occurred concurrently with the dissolution of Mg-Si phases during the solution treatment. The average equivalent area diameter recrystallized grain sizes were $8.6 \mu m$ (Figure 3c) and $39.1 \mu m$ (Figure 3d) for the 30 and 80% cold rolled conditions, respectively. The grain structures were elongated along the extrusion direction and had a recrystallization texture (Figure 4c and 4d) which can be characterized as a mixture of Goss $\{011\}\langle 100\rangle$ and a 45° rotated cube around the normal direction $\{100\}\langle 011\rangle$.

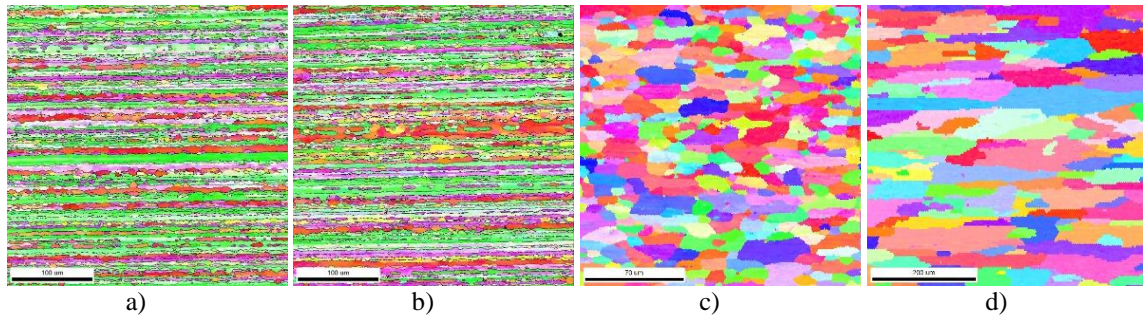


Figure 3. Summary of EBSD results for different grain structures, a) as extruded, b) unrecrystallized after solution treatment, c) recrystallized to grain size of $\approx 9 \mu m$ after cold rolling 80% and solution treated and d) recrystallized to grain size of $\approx 40 \mu m$ after cold rolling 30% and solution treated.

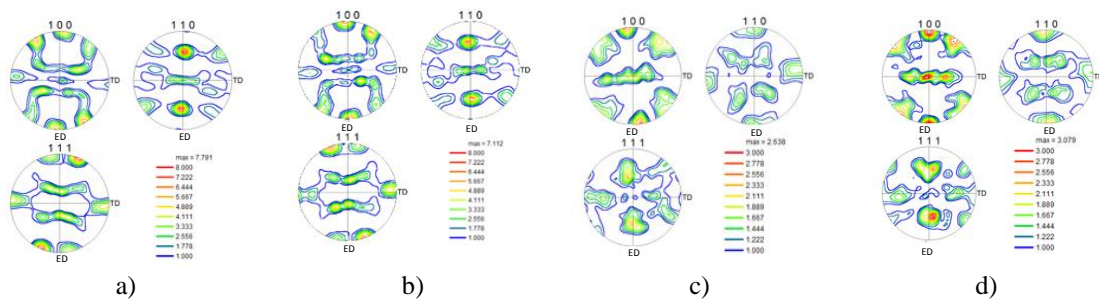


Figure 4. Summary of EBSD measured 001, 110 and 111 pole figure results for different grain structures, a) as extruded, b) unrecrystallized after solution treatment, c) recrystallized to grain size of $\approx 9 \mu m$ after cold rolling 80% and solution treated and d) recrystallized to grain size of $\approx 40 \mu m$ after cold rolling 30% and solution treated.

Figure 5 illustrates the temperature-time data collected from the Gleeble tests showing that controlled cooling could be maintained for the 10, 25, and 80°C/s tests over the temperature range from 560 to 100°C. The results from the thermocouple which was 8 mm away from the centre were also found to be within the desired temperature range, showing minimal temperature gradient within the gauge length of the sample and are not shown in the figure below. The maximum differences in temperature for the unrecrystallized, and recrystallized 40 μm and 9 μm samples were approximately 5, 10 and 25°C respectively. The differences in temperature gradients were due to sample geometry (mainly the difference in thickness due to cold rolling) causing a change in resistivity within the Gleeble.

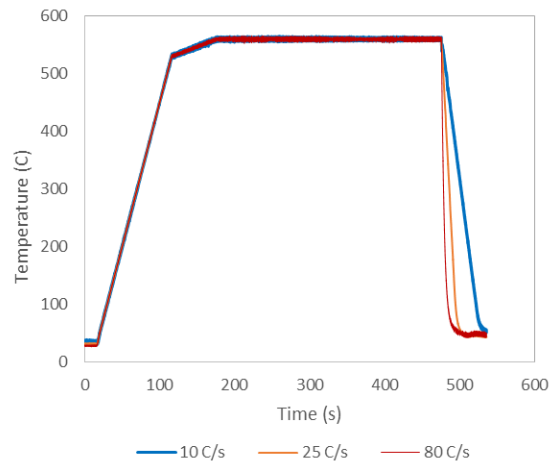


Figure 5. Temperature vs time measurements from the Gleeble tests after solution treatment and helium gas quench.

Figure 6 shows the true stress – true strain curves from the uniaxial tensile tests for the different initial microstructures and cooling rates in the T6 condition. Starting with Figure 6a, it can be observed that there is a strong effect of cooling rate on the yield stress, the large strain work hardening rate and the true fracture stress/strain. The yield stress drops from ≈ 375 MPa to 125 MPa for the water quenched and air cooled samples. In the case of the recrystallized sample with a grain size of ≈ 9 μm or ≈ 40 μm (Figure 6b and 6c), the quench sensitivity was reduced.

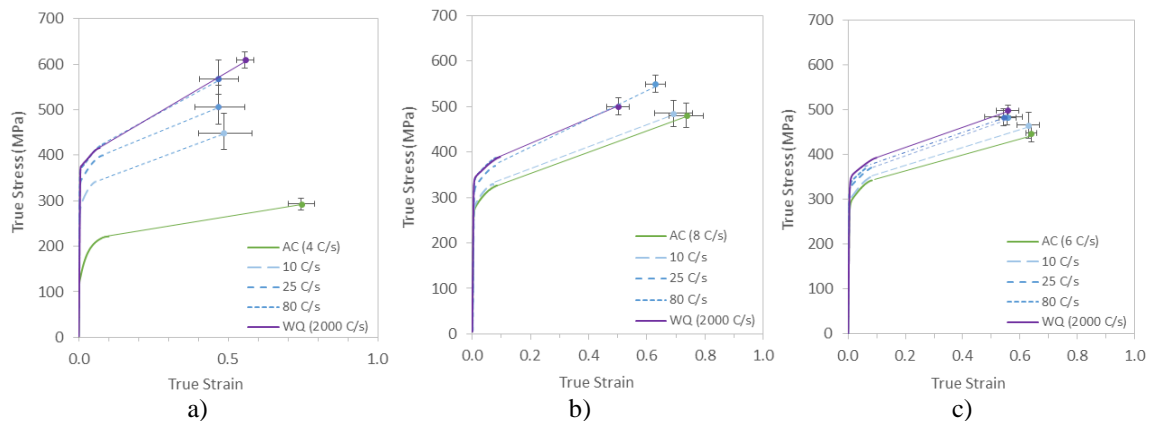


Figure 6. Tensile test results for different microstructures and cooling rates in the T6 condition, a) unrecrystallized, b) recrystallized – 9 μm and c) recrystallized – 40 μm .

Figure 7 shows the FEGSEM secondary electron images for the precipitate structure in samples which had been solution treated and then cooled at the two limiting cooling rates (water quench, $>1000^\circ\text{C/s}$)

and air cooled 2–5°C/s) and aged to T6. The constituent particles show up in these images as the large bright white particles, and the Mg₂Si precipitates can be seen along the grain boundaries or within the grains depending on the quench rate or initial grain structure. Specifically Figure 7a shows that even for the case of the water quenched and aged, unrecrystallized grain structure, some fine Mg-Si precipitates can be observed. This is in contrast to the water quenched, recrystallized samples in Figure 7b and 7c where only constituent and dispersoid particles can be observed, i.e. no Mg-Si precipitates.

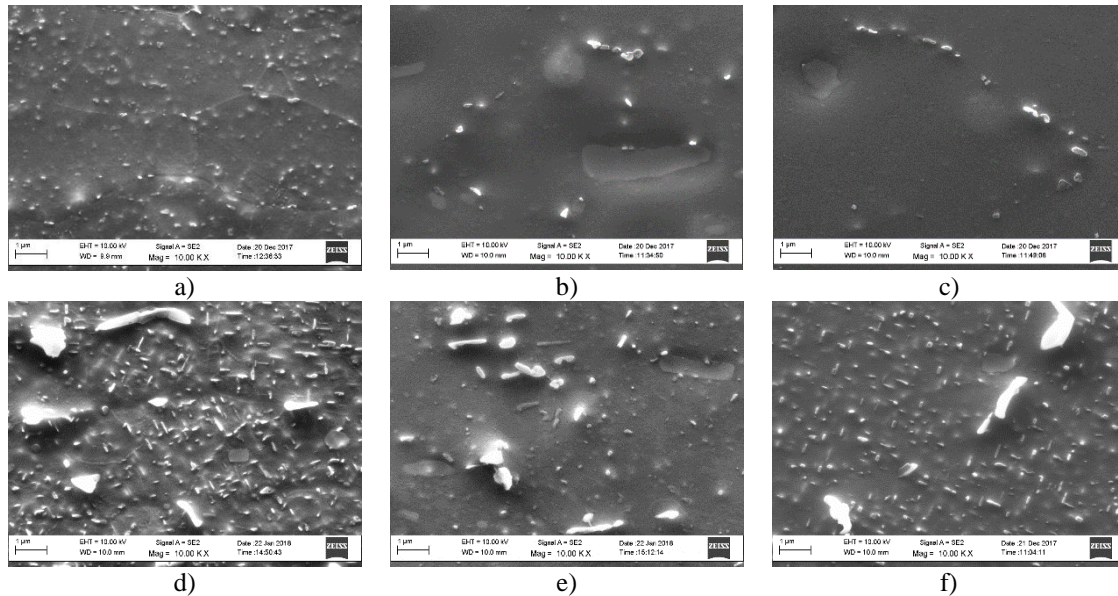


Figure 7. FEGSEM images for different initial grain structures and cooling rates in the T6 condition, a) unrecrystallized, water quench, b) recrystallized 9 μm, water quench, c) recrystallized 40 μm, water quench, d) unrecrystallized, air cooled, e) recrystallized 9 μm, air cooled and f) recrystallized 40 μm, air cooled.

DISCUSSION

Figures 8a and 8b summarize the measured yield stress and the change in yield stress values compared to the as-quenched yield stress as a function of cooling rate for the three different initial microstructures. All three microstructure types exhibit a yield stress decrease with decreasing cooling rate after the solution treatment. In particular, the drop in the T6 yield stress relative to the water quenched value is largest for the unrecrystallized case, i.e. ≈ 250 MPa for the air cooled condition compared to only ≈ 75 MPa for the recrystallized samples. It is speculated that the quench sensitivity of the unrecrystallized material is much higher due to i) the high number of heterogeneous nucleation sites for Mg-Si phases to precipitate on during cooling, i.e. the large area of high angle grain boundaries arising from the deformed grains and the subgrains within the elongated grains and ii) the high dislocation density which can accelerate growth via short circuit diffusion along the dislocation cores. In the case of the recrystallized samples, the dependence of the yield stress on cooling rate presumably comes from the precipitation on dispersoids and grain boundaries as has been previously reported (Dowling & Martin 1976; Strobel et al., 2011; Milkereit & Starink, 2015). Strobel (2013) has proposed that dispersoids will dominate quench sensitivity and that precipitation at grain boundaries is a secondary effect. This would be consistent with the weak effect of the different grain sizes on the cooling rate dependence of the yield stress. Finally, the FEGSEM images shown in Figure 7 also show that the precipitation of Mg-Si phases is qualitatively more extensive in the unrecrystallized case. This would be consistent with the larger loss of yield stress in the unrecrystallized condition compared to the recrystallized conditions.

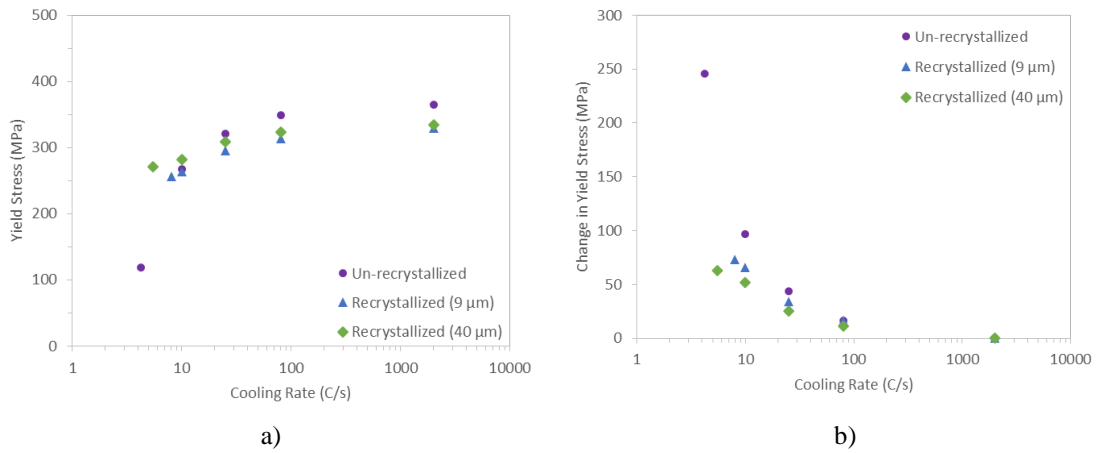


Figure 8. Effect of cooling rate on the T6 strength of the alloys for different initial microstructures, a) yield stress and b) change in yield stress, i.e. yield stress at a given cooling rate subtracted from the water quenched value.

Finally, Figure 9 summarizes the effect of cooling rate on the true fracture stress and true fracture strain. In Figure 9a, it can be observed that the true fracture stress is only weakly dependent on cooling rate for the recrystallized alloys, although the true fracture stress for the 9 μm is slightly higher (485–550 MPa) compared to that of the 40 μm sample (435–510 MPa). On the other hand, the results for the unrecrystallized microstructure show a strong dependence on cooling with the true fracture stress dropping from ≈600 MPa in the water quenched sample to ≈250 MPa in the air cooled case. This would be consistent with the simple model of Evensen and co-workers (Evensen et al., 1975) who proposed that the stress on the grain boundary would depend on grain size similar to the Hall-Petch effect. It would also suggest that the intrinsic strength of the grain boundary is only weakly dependent on cooling rate. Turning to the true fracture strain, Figure 9b shows that the recrystallized samples exhibit larger true strain to fracture compared to the unrecrystallized sample with the finer grain size sample having larger true strain to failures values than the larger grain size samples. The explanation for the details of these differences requires further investigation.

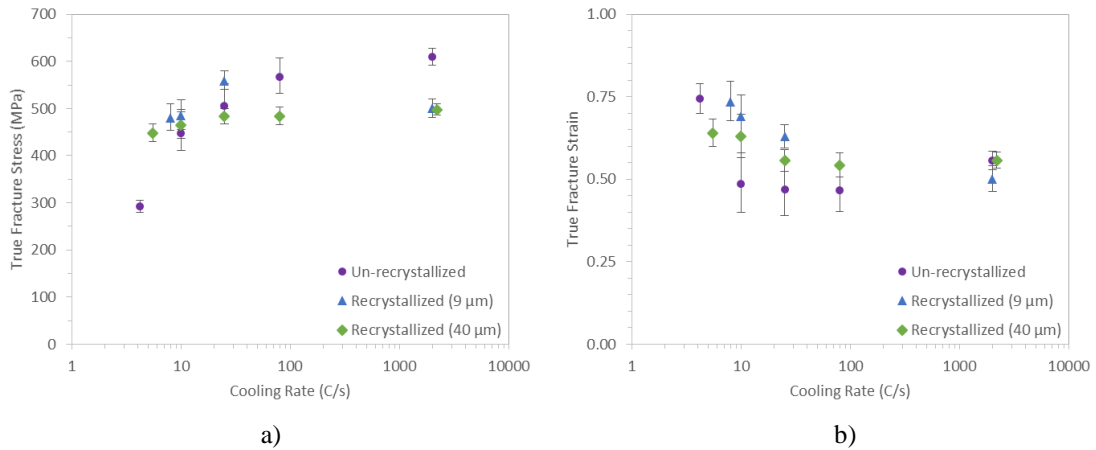


Figure 9. Fracture properties for the different microstructures in the T6 condition as function of cooling rate, a) true fracture stress and b) true fracture strain.

SUMMARY

In summary, a methodology has been developed using the Gleeble 3500 thermomechanical simulator to conduct solution treatment and cooling tests with a wide range of cooling rates. The samples from these simulations are suitable for conducting tensile tests to evaluate mechanical properties. In the current work, the influence of post solution treatment cooling rate for different initial microstructures was studied with one unrecrystallized and two recrystallized microstructures (in the T6 aged temper). In the case of the unrecrystallized microstructure, it was found that the yield stress decreased by ≈ 250 MPa and true fracture stress decreased by ≈ 350 MPa as the cooling rate was decreased from >1000 to $<10^\circ\text{C/s}$. In contrast, the recrystallized microstructures showed a much smaller dependence of the yield stress (< 75 MPa) and an almost cooling rate independent true fracture stress, albeit the true fracture stress was approximately 50 MPa lower for the 40 vs 9 μm grain size materials.

The effect of cooling rate on the mechanical properties has been rationalized in terms of the precipitation of Mg-Si phases during cooling and FEGSEM observations are qualitatively in agreement. The strong dependence of mechanical behaviour for the unrecrystallized material is speculated to arise from the high density of heterogeneous nucleation sites, e.g. elongated high angle grain boundaries and subgrains within the grains, and the dislocation network which aid the nucleation and growth of Mg-Si phases during cooling compared to the recrystallized materials. Future work is needed to quantify the precipitation during cooling for different cooling rates.

ACKNOWLEDGMENTS

The authors would like to acknowledge the financial support of the Ford Motor Company, Rio Tinto Aluminium and NSERC Canada. The assistance of Zhijun Zhang (post-doctoral fellow) and Mojtaba Mansouri (PhD student) from the Microstructure Group at UBC is gratefully acknowledged, in particular for their help with the EBSD work.

REFERENCES

- Dowling, J. M. & Martin J. W. (1976). The influence of Mn additions on the deformation behaviour of an Al-Mg-Si alloy. *Acta Metall.* 24: 1147-1153.
- Evensen, J. D., Ryum, N. et al. (1975). The intergranular fracture of Al-Mg-Si alloys. *Mat. Sci. Eng.* 18: 221-229.
- Liu, C. (2017). Microstructure evolution during homogenization and its effect on the high temperature deformation behaviour in AA6082 based alloys *PhD. Thesis, Department of Materials Engineering.* Vancouver, BC, The University of British Columbia. Ph.D.
- Lodgaard, L. & Ryum, N. (2000). Precipitation of dispersoids containing Mn and/or Cr in Al-Mg-Si alloys. *Mat. Sci. Eng. A* 283(1-2): 144-152.
- Milkereit, B. & Starink, M.J. (2015). Quench sensitivity of Al-Mg-Si alloys: A model for linear cooling and strengthening. *Mater. Design* 76: 117-129.
- Strobel, K. (2013). *Quench Sensitivity in 6xxx Series Aluminium Alloys, Ph.D Thesis,* Monash University.
- Strobel, K., Easton, M. A. et al. (2011). Relating quench sensitivity to microstructure in 6000 series aluminium alloys. *Mater. Trans.* 52: 914-919.
- Vasudevan, A. K. & Doherty, R. D. (1987). Grain boundary ductile fracture in precipitation hardened aluminum alloys. *Acta Metall.* 35: 1193-1219.